Electronic Supplementary Material (ESI) for Journal of Materials Chemistry C.

Extreme-Modulation of Liquid Crystal Viscoelasticity via Altering Ester Bond Direction

Wentao Tang,[a] Minghui Deng,[a] Junichi Kougo[a,b], Li Ding,[c] Xiuhu Zhao,[a] Yuki Arakawa,*[d] Kenta Komatsu,[d] Hideto Tsuji[d] and Satoshi Aya*[a,b]

[a] South China Advanced Institute for Soft Matter Science and Technology (AISMST), School of Molecular Science and Engineering, South China University of Technology, Guangzhou 510640, China

[b] Guangdong Provincial Key Laboratory of Functional and Intelligent Hybrid Materials and Devices, South China University of Technology, Guangzhou 510640, China

[c] School of Materials Science and Engineering (International School of Advanced Materials), South China University of Technology, Guangzhou 510641, China

[d] Department of Applied Chemistry and Life Science, Graduate School of Engineering, Toyohashi University of Technology, Toyohashi, 441-8580 Japan

* Corresponding Author. E-mail: satoshiaya@scut.edu.cn, E-mail: arakawa@tut.jp

Contents

1. Dielectric spectroscopy

The dielectric spectroscopy was made by using a multichannel electrochemical workstation (VMP3 Potentiostat, BioLogic). As shown in Fig. S9, a large dielectric relaxation was observed for COO_4 and OCO_4 molecules (also for all the other homologues) with the relaxation strength, $\delta\varepsilon$, of over 100. Similar relaxation process, but with small $\delta\varepsilon$, was observed previously, and assigned to a goldstone mode that corresponds to the long-scale fluctuations of the azimuthal angle of the local nematic director along the coarse-grained the coarse grained director.[S1-S3] The correlation length of the precession fluctuation can be estimated by using a non-stationary solution of the Smoluchowski equation.[S1] The correlation length is written as $\delta z^2 \approx D/q^2\omega$. D, q and ω are the orientational di□usion coe□cient, wavenumber of the heliconical structure and the frequency. We used D=10^9 s^{-1}, q from Ref. S4 and ω from the measured dielectric spectrum (e.g. Fig. S9) for calculating the correlation length δz. Fig. S10 demonstrates COO_4 exhibits considerably longer correlations than others. With increasing the number of the carbon spacer in COO_n, the correlation length decreases to nearly similar to that of OCO_n.

2. Switching time tuning by mixing

To seek the possibility for tuning the viscoelastic properties in a wide range of values, we studied the LCD electro-optical characteristics by mixing COO_4 and OCO_4 molecules. We confirmed the solubility of COO_4 in OCO_4 very nice independent on the weight ratio. The phase diagram is shown in Fig. 3(a). Strikingly, the increasing of the weight of COO_4 in OCO_4 allows us for extremely modulate the switching time, continuously going from c.a. 0.1 s (pure OCO_4) up to several hundreds of seconds (pure COO_4). Fig. S11 represents the temperature dependence of off-switching time in various mixtures with different mixing ratio of COO_4 by weight.

3. Switching time for COO_n and OCO_n homologs (n = 8 and 10)

As discussed in the manuscript, decreasing the carbon number in the spacer causes the slow-down of their dynamics, suggesting the stronger molecular packing at longer flexible spacers. Here we show the temperature dependence of off-switching time in COO_n and OCO_n (n = 8 and 10) in Fig. S12. As shown in the figure, a decrease in the off-switching time was observed in COO homologs with increasing carbon number of spaces. Their off-switching time is in the order of hundred seconds, which is still one order longer than that in OCO_n. Based on the Arrenius plots, the rotation activation energy for COO_{10} (0.52ev) is about two times of that in OCO_{10}. (0.34ev) while the rotation activation energy for COO_6 (1.61ev) is around four times magnitude for OCO_6 (0.42ev). It is revealed that the activation energy of COO_n (n = 8 and 10) is comparable with thoes in OCO_n (n = 4 and 6). Thereby, reducing the carbon number in the spacer results in the decrease of the activation energy in the COO_n. This result is well consistent with the dielectric measurements.

4. Supporting figures

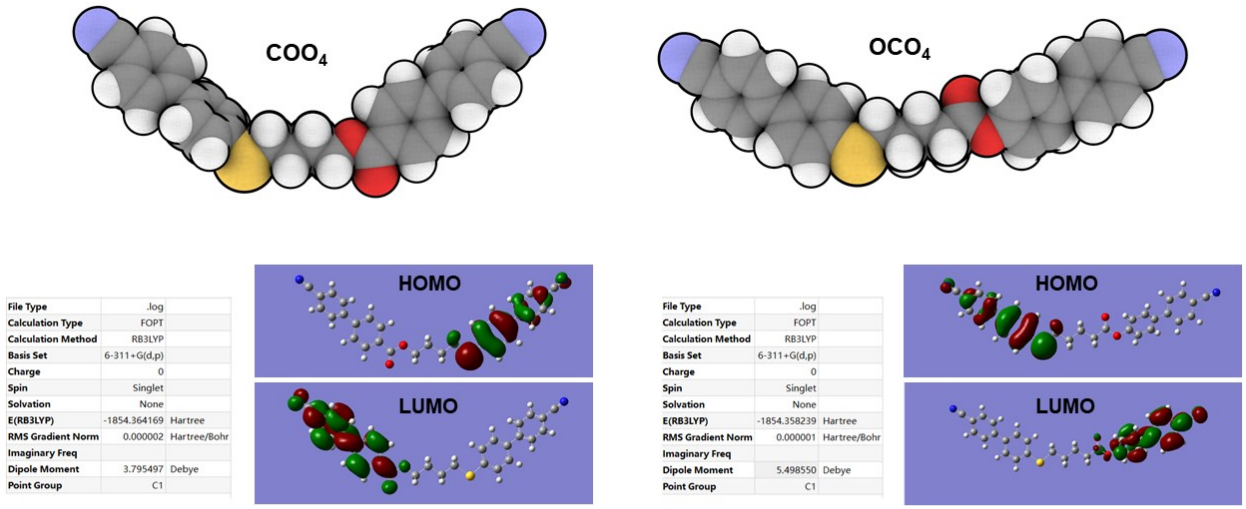

File Type	.log	
Calculation Type	FOPT	
Calculation Method	RB3LYP	
Basis Set	6-311+G(d,p)	
Charge	0	
Spin	Singlet	
Solvation	None	
E(RB3LYP)	-1854.364169	Hartree
RMS Gradient Norm	0.000002	Hartree/Bohr
Imaginary Freq		
Dipole Moment	3.795497	Debye
Point Group	C1	

File Type	.log	
Calculation Type	FOPT	
Calculation Method	RB3LYP	
Basis Set	6-311+G(d,p)	
Charge	0	
Spin	Singlet	
Solvation	None	
E(RB3LYP)	-1854.358239	Hartree
RMS Gradient Norm	0.000001	Hartree/Bohr
Imaginary Freq		
Dipole Moment	5.498550	Debye
Point Group	C1	

Fig. S1. Summary of DFT calculation at B3LYP-G3/6-311+G(d,p) basis for COO_4 and OCO_4 molecules.

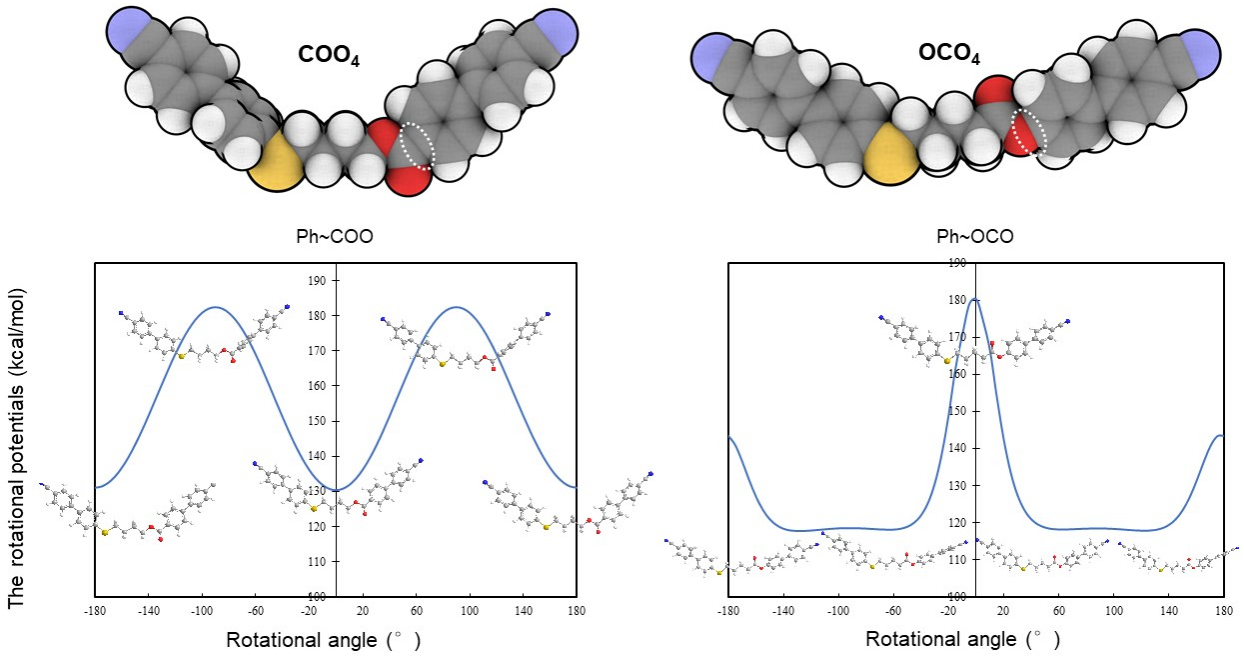

Fig. S2. The rotational potentials about Ph–C or Ph–O bonds (represented by dotted circles in the upper space filling representations for COO_4 and OCO_4, respectively) as a function of the rotation angle.

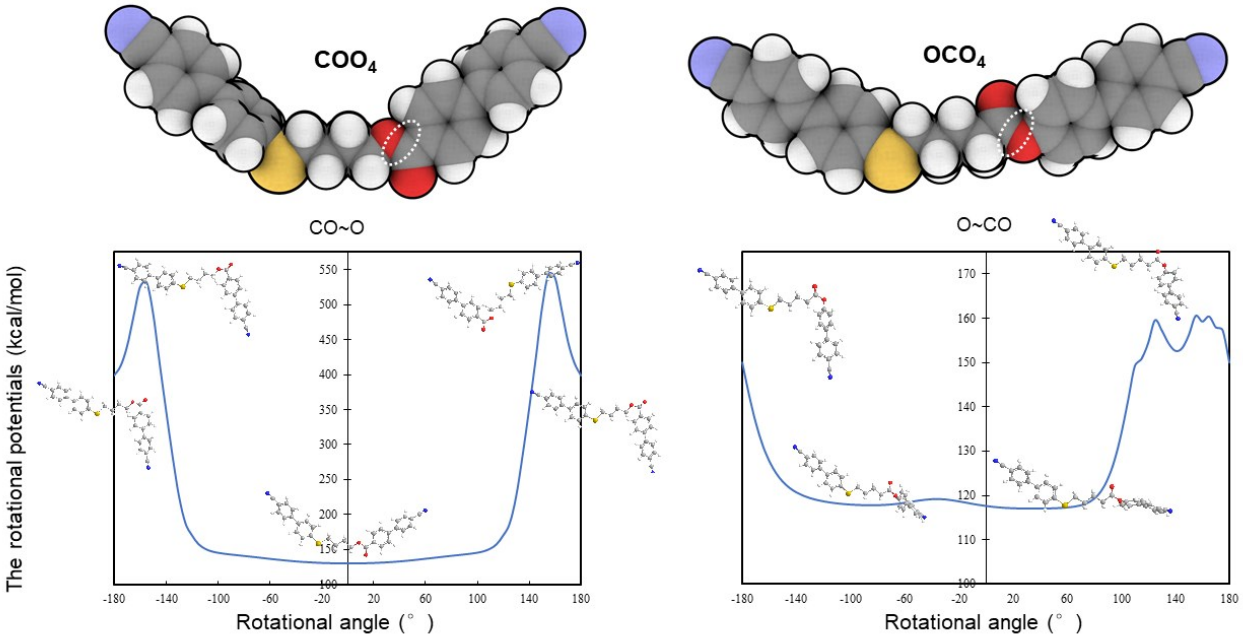

Fig. S3. The rotational potentials about C–O or O–C bonds (represented by dotted circles in the upper space filling representations for COO_4 and OCO_4, respectively) as a function of the rotation angle.

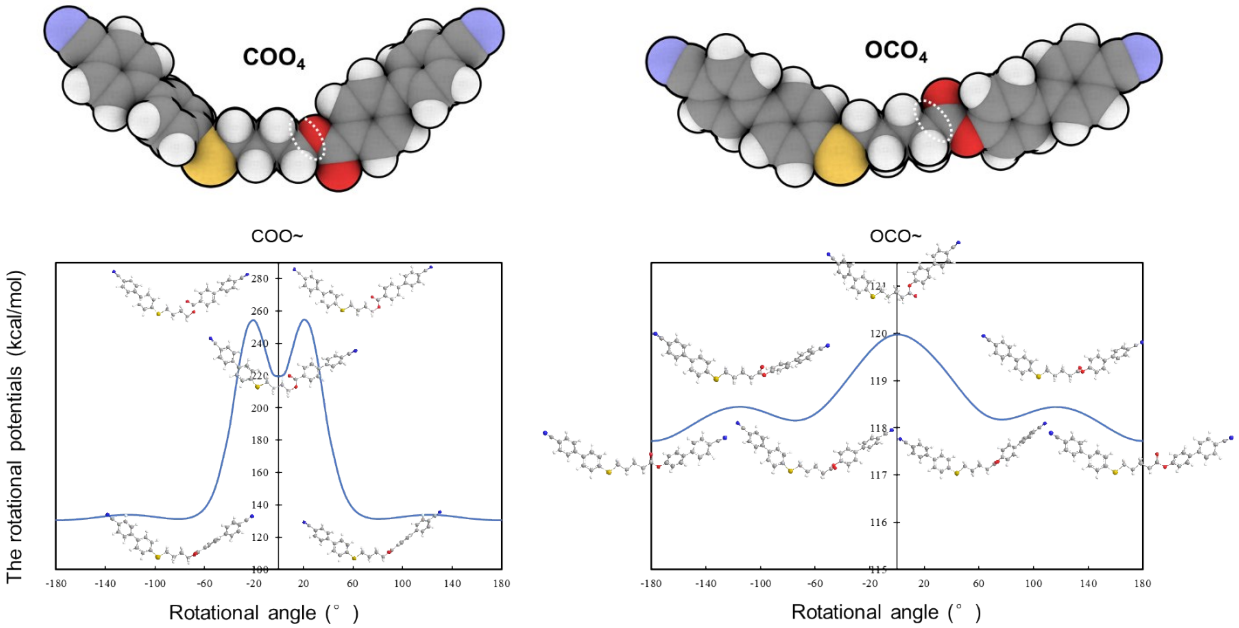

Fig. S4. The rotational potentials about O–C or C–C bonds (represented by dotted circles in the upper space filling representations for COO_4 and OCO_4, respectively) as a function of the rotation angle.

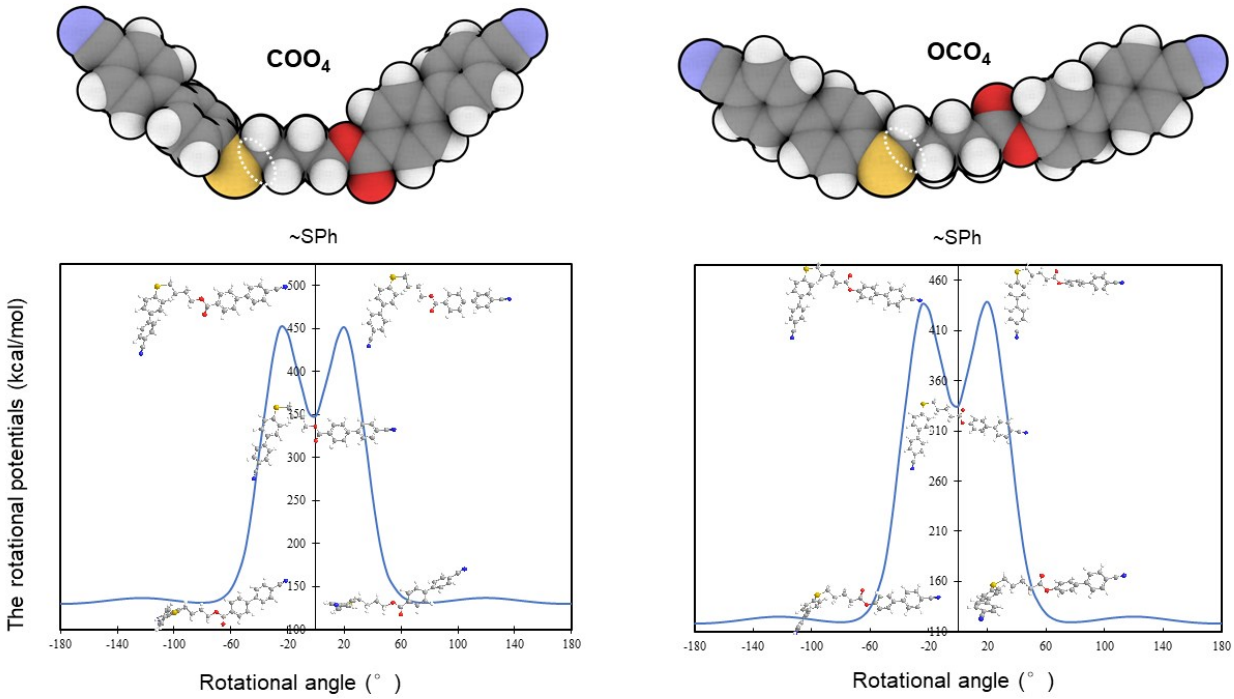

Fig. S5. The rotational potentials about –SC bonds (represented by dotted circles in the upper space filling representations for COO_4 and OCO_4) as a function of the rotation angle.

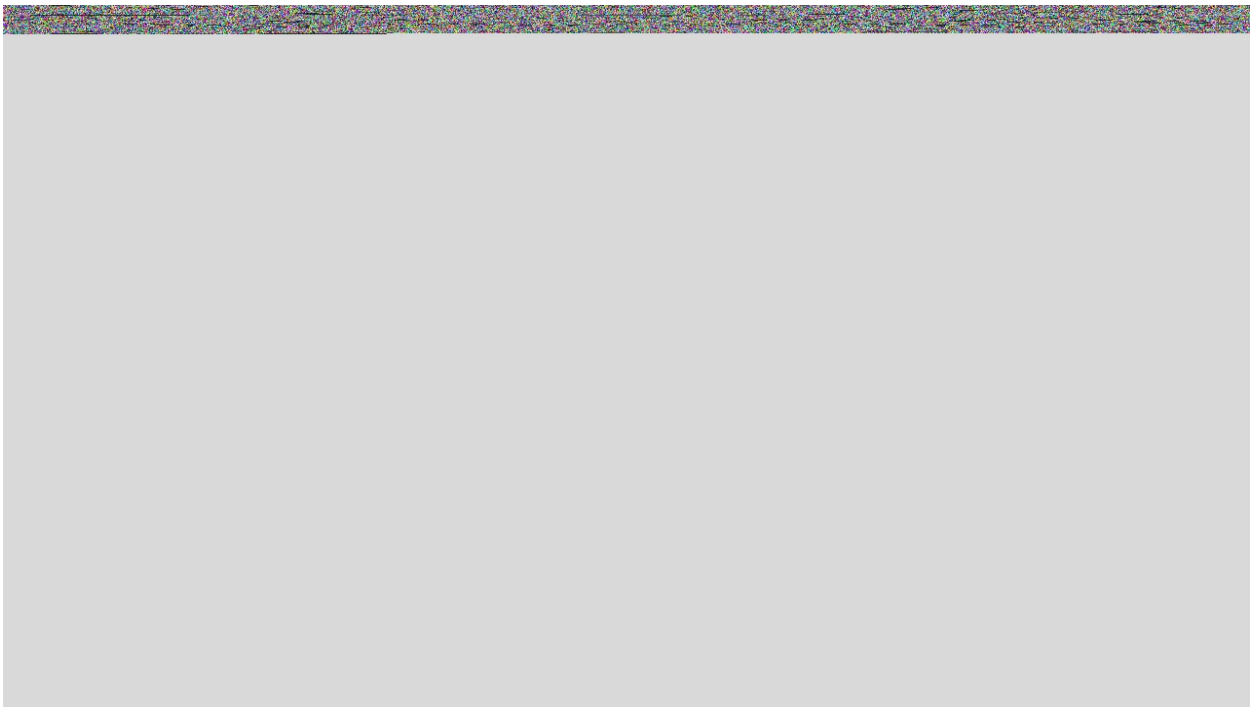

Fig. S6. The rotational potentials about S–C bonds (represented by dotted circles in the upper space filling representations for COO_4 and OCO_4) as a function of the rotation angle.

Fig. S7. (a-f) Stripe textures of COO_4 and OCO_4 molecules are presented at the different thicknesses of the samples. (g) The temperature dependence of the stripe periodicity is shown as a function of temperature.

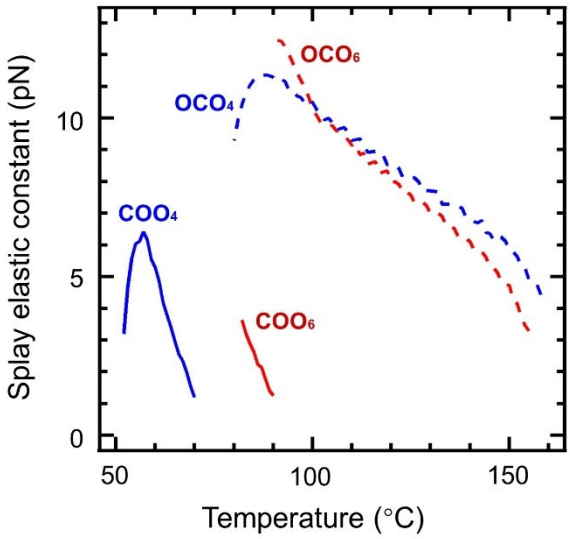

Fig. S8. Temperature dependencies of the splay elastic constant of the N phase in the four molecules, COO_4, OCO_4, COO_6 and OCO_6.

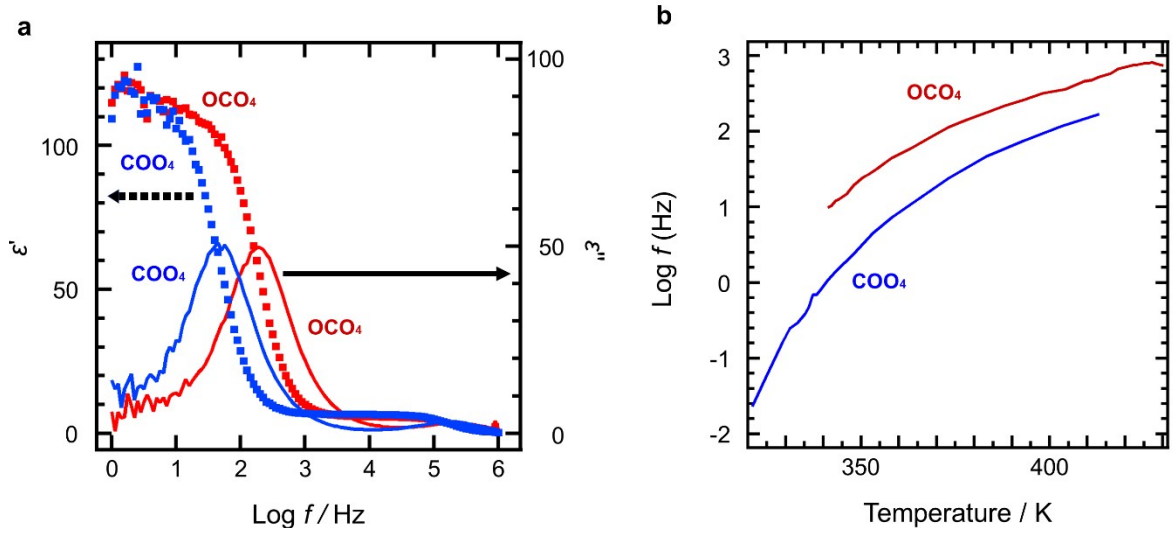

Fig. S9. Dielectric spectroscopy of COO_4 and OCO_4: (a) The real and imaginary dielectric permittivity. The full squares show the real dielectric permittivity data. The solid lines show the imaginary dielectric permittivity data.; (b) The temperature dependence of the relaxation frequency of the slowest relaxation mode, m4.

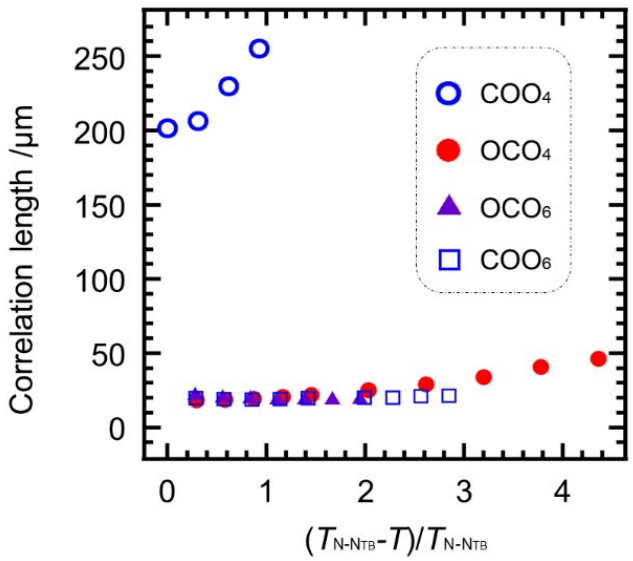

Fig. S10. The correlation lengths of the fluctuation of the azimuthal angle of the local director for COO_4, OCO_4, COO_6 and OCO_6 as a function of a scaled temperature.

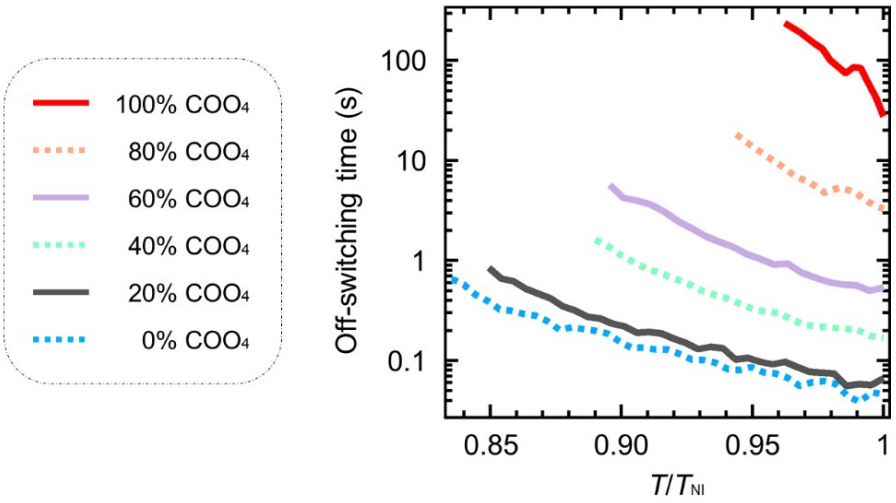

Fig. S11. The temperature dependencies of the off-switching time for COO_4-OCO_4 mixtures at different weight ratios of COO_4.

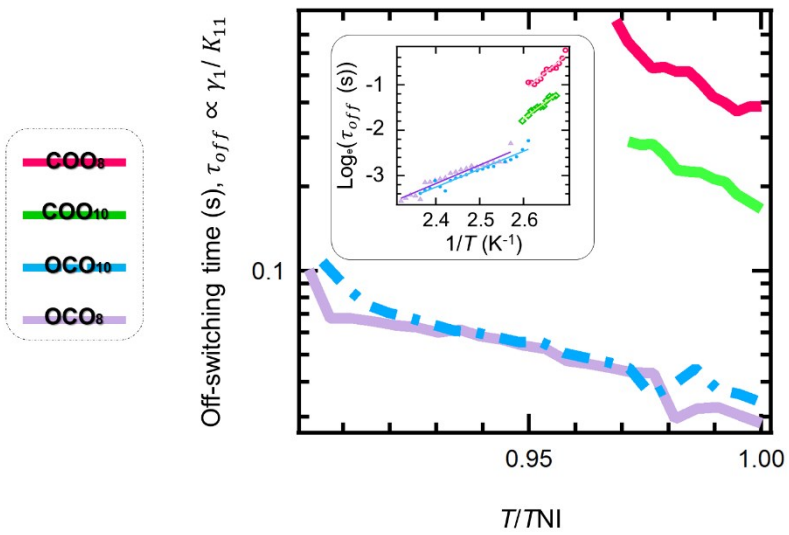

Fig. S12. The temperature dependencies of the off-switching time for COO_n and OCO_n (n = 8 and 10). The inset demonstrates the corresponding Arrhenius plot. T_{NI} is the transition temperature between the N and the isotropic liquid state.

References

S1. K. Merkel, A. Kocot, C. Welch and G. H. Mehl, Soft Modes of the Dielectric Response in the Twist-Bend Nematic Phase and Identification of the Transition to a Nematic Splay Bend Phase in the CBC7CB Dimer, *Phys. Chem. Chem. Phys.*, 2019, **21**(41), 22839–22848.

S2. K. Merkel, A. Kocot, J. K., Vij, G. Shanker, Distortions in Structures of the Twist Bend Nematic Phase of a Bent-Core Liquid Crystal by the Electric Field, *Phys. Rev. E*, 2018, **98**(2), 1–8.

S3. K. Merkel, C. Welch, Z. Ahmed, W. Piecek and G. H. Mehl, Dielectric Response of Electric-Field Distortions of the Twist-Bend Nematic Phase for LC Dimers, *J. Chem. Phys.*, 2019, **151**(11), 114908.

S4. Y. Arakawa, K. Komatsu, J. Feng, C. Zhu and H. Tsuji, Distinct Twist-Bend Nematic Phase Behaviors Associated with the Ester-Linkage Direction of Thioether-Linked Liquid Crystal Dimers, *Mater. Adv.*, 2021, **2**(1), 261–272.